

High resolution TCSPC lifetime imaging

Wolfgang Becker^a, Axel Bergmann^a,
Christoph Biskup^b, Laimonas Kelbauskas^b, Thomas Zimmer^b, Nikolaj Klöcker^c,
Klaus Benndorf^b

^aBecker & Hickl GmbH, Nahmitzer Damm 30, D-12277 Berlin, Germany

^bFriedrich-Schiller-Universität, Institut für Physiologie II, Teichgraben 8, D-07740 Jena,
Germany

^cAlbert-Ludwigs-Universität Freiburg, Institut für Physiologie, D-79104 Freiburg, Germany

ABSTRACT

Time-correlated single photon counting (TCSPC) fluorescence lifetime imaging in laser scanning microscopes can be combined with a multi-detector technique that allows to record time-resolved images in several wavelength channels simultaneously. The technique is based on a multi-dimensional histogramming process that records the photon density versus the time within the fluorescence decay function, the x-y coordinates of the scanning area and the detector channel number. It avoids any time gating or wavelength switching and therefore yields a near-ideal counting efficiency. We show an instrument that records dual wavelength lifetime images with up to 512 x 512 pixels, and single wavelength lifetime images with up to 1024 x 1024 pixels. It resolves the components of double-exponential decay functions down to 30 ps, and works at the full scanning speed of a two-photon laser scanning microscope. The performance of the instrument is demonstrated for simultaneous lifetime imaging of the donor and acceptor fluorescence in CFP / YFP FRET systems and for tissue samples stained with several fluorophores.

1. INTRODUCTION

In the last years fluorescence lifetime imaging (FLIM) has become an established technique to investigate energy transfer processes in cells. FLIM has been used to exploit the environment-dependent lifetime of fluorophores as a marker function, to measure the pH value, the oxygen concentration or concentrations of physiologically relevant ions [1-4]. In FRET experiments the lifetimes are directly related to the energy transfer from the donor to the acceptor [5,6]. FLIM can also be used to distinguish between different fluorophores [7,17,18]. In particular, the fluorescence lifetime helps to distinguish between different natural fluorophores with their often overlapping and poorly defined fluorescence spectra [8,9].

Simultaneously, confocal (CLSM) and two-photon laser scanning microscopes (TPLSM) caused a revolution in cell imaging [10-15]. The capability of high contrast fluorescence imaging, depth resolution, and deep tissue imaging make these instruments superior to conventional microscopes.

All lifetime imaging techniques - the single detector modulation technique [16-18], modulated image intensifiers [19-21], gated image intensifiers [22,23], multi-gate photon counting [24,25], and time-correlated single photon counting (TCSPC) [5,26-28] have been used in combination with laser scanning microscopes. However, only the single-detector modulation technique, multi-gate photon counting and TCSPC can exploit the capability of CLSMs and TPLSMs to deliver clear images of deep tissue layers.

Unfortunately the fluorescence decay functions in practical FLIM applications are usually not single exponential. Natural fluorophores often have several decay components by themselves, and the variable local environment may change the lifetime of different molecules in a different way. In FRET experiments the FRET intensity depends on the random distance and orientation of the donor and acceptor molecules, which makes the donor lifetime clearly multi-exponential [5]. Deriving the FRET efficiency or intermolecular distances from a single exponential decay approximation may lead to wrong results.

Another basic problem of all FLIM techniques in microscopy is to get a sufficiently large number of photons from a small sample volume. Although acceptable steady state images can be obtained with less than 100 photons per pixel, even rough single exponential decay analysis requires several 100 photons. High accuracy single exponential analysis requires several 1000 photons, and double exponential decay analysis some 10.000 to 100.000 photons per

pixel [29]. Unfortunately the number of photons that can be obtained from a sample is limited by photobleaching. The problem is particularly severe for two-photon excitation where photobleaching is highly nonlinear [30]. Therefore, a FLIM technique for multi-exponential decay analysis does not only need a sufficiently high intrinsic time resolution and accuracy but also a high counting efficiency. Although all FLIM techniques are more or less capable to resolve multi-exponential decays only TCSPC can be considered a standard technique for multi-exponential decay analysis in scanning microscopes. We will show that the TCSPC imaging technique has a superior counting efficiency, resolves lifetimes down to a few 10 ps, allows for multi-exponential decay analysis, and is compatible with the fast scan rates of modern CLSMs and TPLSMs. Moreover, TCSPC imaging is able to record images in different wavelength intervals simultaneously. Multi-wavelength operation increases the efficiency of TCSPC imaging even beyond the widely accepted theoretical limit given in [34].

2. MULTI-WAVELENGTH TCSPC IMAGING

Traditional time-correlated single photon counting is based on the excitation of the sample with a high-repetition rate pulsed light source, the detection of single fluorescence photons, and the build-up of a histogram of the photon detection times. The result is the distribution of the photon density versus time, i.e. the fluorescence decay curve. Compared to traditional TCSPC setups [26,27,31] the maximum photon count rate has been increased dramatically by using high repetition rate Titanium-Sapphire lasers and a new analog-to-digital conversion technique [32]. For use in laser scanning microscopes the technique has been extended to the build-up of a three-dimensional photon density pattern versus the time in the decay curve and the coordinates of the scanning area [28].

The TCSPC imaging technique can be used with several detectors working in different wavelength intervals. The technique works both with a multichannel PMT [33] and with several individual PMTs or MCP-PMTs [32]. It makes use of the fact that the detection of several photons in different detector channels in one laser period is unlikely. Therefore, the single photon pulses from all detector channels can be combined into a common photon pulse line and sent through the normal time measurement procedure of the TCSPC module.

The principle of the used detector electronics is shown in fig. 1. The output of each PMT channel is connected to a discriminator. When the PMT detects a photon the corresponding discriminator triggers and sends a pulse to the subsequent encoding logic. The encoder delivers the number of the PMT channel that detected the photon. The channel number is used as an additional dimension in the multi-dimensional histogramming process of the TCSPC imaging technique. In the unlikely case that several detectors deliver output pulses in the same laser period the encoder delivers a 'don't count' signal that suppresses the recording of the event in the TCSPC module. The technique can reasonably be used for up to four individual ultra-fast MCP-PMTs or one 16 channel or 32 channel multi-anode PMT.

The principle of the multi-detector TCSPC imaging technique is shown in fig. 2. The recording electronics consists of a time measurement channel, a scanning interface, a detector channel register, and a large histogram memory. The time measurement channel contains the usual TCSPC building blocks (CFDs, TAC, ADC) in the 'reversed start-stop' configuration. For each photon, it determines the detection time (t) with respect to the next laser pulse. The scanning interface is a system of counters which receive the scan control signals (frame sync, line sync and pixel clock) from the microscope. It determines the current location (x and y) of the laser spot in the scanning area. Synchronously with the detection of a photon, the detector channel number (n) for the current photon is read into the detector channel register. If the light is split into different wavelength intervals in front of the detectors n represents the wavelength of the detected photon.

The obtained values for t, x, y and n are used to address the histogram memory in which the distribution of the photons over time, wavelength, and the image coordinates builds up. The result is a four dimensional data structure

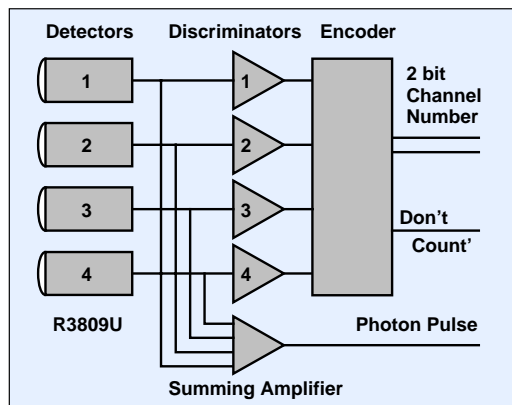


Fig. 1: Principle of detector electronics for TCSPC multi-detector operation

that contains separate blocks for the different wavelength intervals. Each block can be regarded as an image containing a full fluorescence decay curve in each pixel.

The data acquisition runs at any desired scanning speed of the microscope. The data acquisition can be repeated as often as necessary to collect enough photons. Due to the synchronisation via the scan clock pulses, the regular zoom and image rotation functions of the microscope act automatically on the TCSPC recording and can be applied in the usual way.

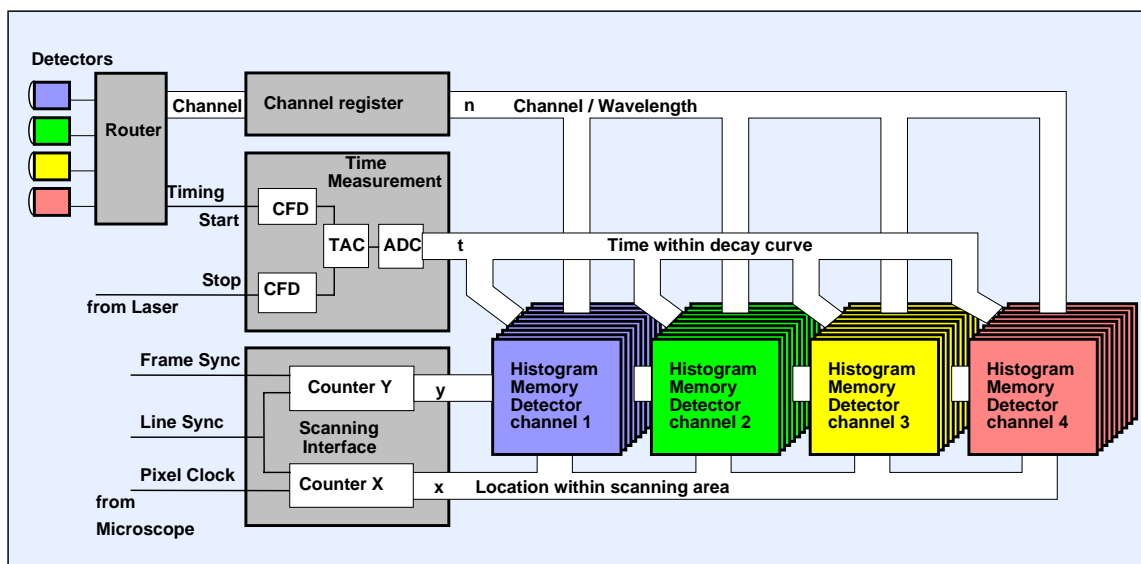


Fig. 2: Multi-detector TCSPC imaging

It should be pointed out that the histogramming process does not use any time gating or wavelength scanning. Therefore, the method yields a near perfect counting efficiency and a maximum signal to noise ratio for a given fluorescence intensity and acquisition time. Due to the short dead time of the TCSPC imaging electronics (125 ns) there is virtually no loss of photons for count rates up to a few $10^5/s$ as they are typical for cell imaging.

To characterise the efficiency of a recording technique both the 'counting efficiency' and the 'figure of merit' [34] can be used. The counting efficiency, E , is the ratio of the number of recorded photons to the number of detected photons. The figure of merit, F , is the ratio of the signal-to-noise ratios of an ideal technique recording all detected photons and the technique under consideration.

$$E = \frac{N_{\text{recorded}}}{N_{\text{detected}}} \quad F = \frac{SNR_{\text{ideal}}}{SNR_{\text{actual}}} \quad F = \frac{1}{E^2}$$

Fig. 3 shows the counting efficiency and the figure of merit as a function of the detector count rate for commonly used FLIM techniques. The values for the modulation techniques and the gated image intensifier are according to [35], the values for the multi-gate photon counting technique were taken from [36]. The TCSPC values were calculated for a dead time of 125 ns. The efficiency of TCSPC is almost independent of the fluorescence lifetime down to the full width at half maximum (FWHM) of the instrument response function (IRF). However, it decreases at high count rates because some of the detected photons are lost in the system dead time. Nevertheless, TCSPC beats all the other techniques for efficiency up to detector count rates of 4 MHz. This count rate is higher than the maximum count rate that can be obtained from an R3809U MCP without exceeding the maximum permitted output current. The counting efficiency of dual-detector TCSPC imaging is even better than the theoretical limit of [34]. This result is explained by the fact that the reference for the counting efficiency and the figure of merit is an ideal single channel recording device. The two channels of a dual-detector TCSPC device ideally record twice as much photons so that the efficiency is correspondingly better.

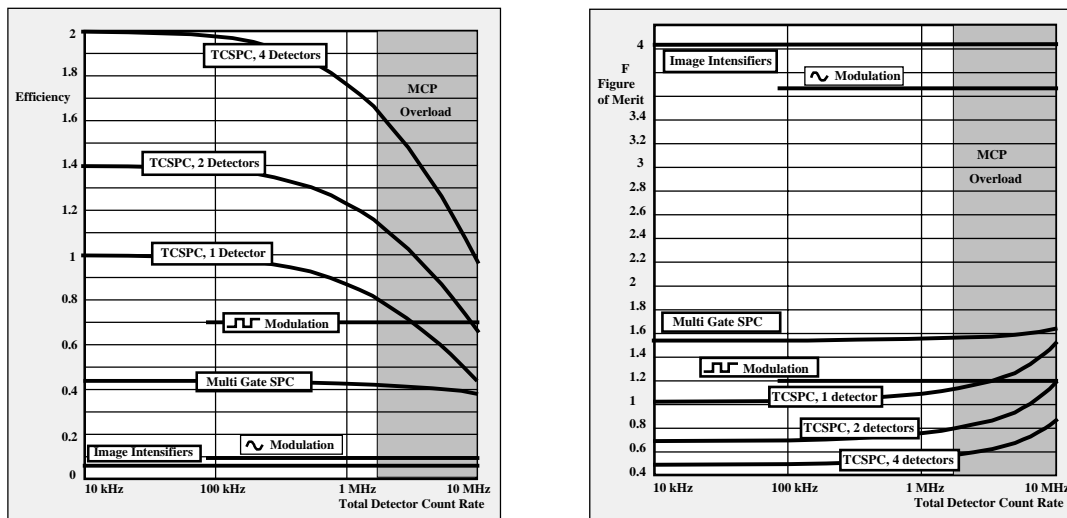


Fig. 3: Counting efficiency and figure of merit F of TCSPC imaging compared to other techniques
 F is the ratio of theoretical SNR to obtained SNR, F=1 means ideal SNR

3. MICROSCOPE SETUP

The general setup of the FLIM microscope is shown in fig. 4. For the measurements presented below we used a Zeiss LSM 510 NLO two-photon laser scanning microscope in the Axiovert 200 version. An excitation wavelength of 860 nm was used for all experiments described in this paper. The non-descanned fluorescence signal from the sample was fed out of the rear port of the Axiovert. A dual detector assembly with a dichroic beamsplitter and two Hamamatsu R3809U MCPs was attached to this port. BG39 laser blocking filters and bandpass filters were inserted directly in front of the detectors. For all measurements presented below we used a 510 nm dichroic (FT510, Zeiss) and bandpass filters with 480 ± 15 nm and 535 ± 13 nm transmission wavelength from Omega Optical, Brattleboro. The filters were selected to detect the fluorescence of the CFP and the YFP, respectively.

Photon counting detectors, particularly MCP-PMTs, can easily be damaged or destroyed by overload. Even when an MCP or PMT is switched off the cathode performance is impaired temporarily if the cathode is exposed to a high light intensity [37]. In all microscopes the microscope lamp is a potential source of detector damage. Thus, a simple operator error can destroy one or several FLIM detectors. Even daylight leaking through the sample into the detection path can cause severe detector overload. The problem is particularly severe in two-photon microscopes with non-descanned detection because the detection optics collects the light from a large area of the sample. In these instruments the light from the lamp can be so strong that the detector is jeopardised even when its operating voltage is switched off. Therefore, a FLIM system has to include suitable overload protection for the detectors.

We used a shutter in front of the detector assembly. The shutter is closed when the maximum detector output current - 100 nA for the R3809U MCP - is exceeded or when a photodiode in front of the shutter detects a dangerous intensity level. Thus, the shutter closes when overload occurs and cannot be opened as long as a potential overload situation persists. The detector / shutter assembly is shown in fig. 5. A similar setup with two shutters can be used for LSM 510 microscopes with the Zeiss NDD switch box installed (fig. 6).

The single photon pulses from the two R3809U detectors are fed into the HRT-41 router [38]. For each detected photon, the router delivers a timing pulse and a 'routing' bit that indicates in which PMT the photon was detected. These signals are connected to the SPC-830 TCSPC imaging module [39]. The reference signal for the time measurement is obtained from the reference photodiode of the Titanium-Sapphire laser. The imaging process in the SPC-830 module is synchronised with the scanning process via the frame sync, line sync and pixel sync signals from the microscope control box.

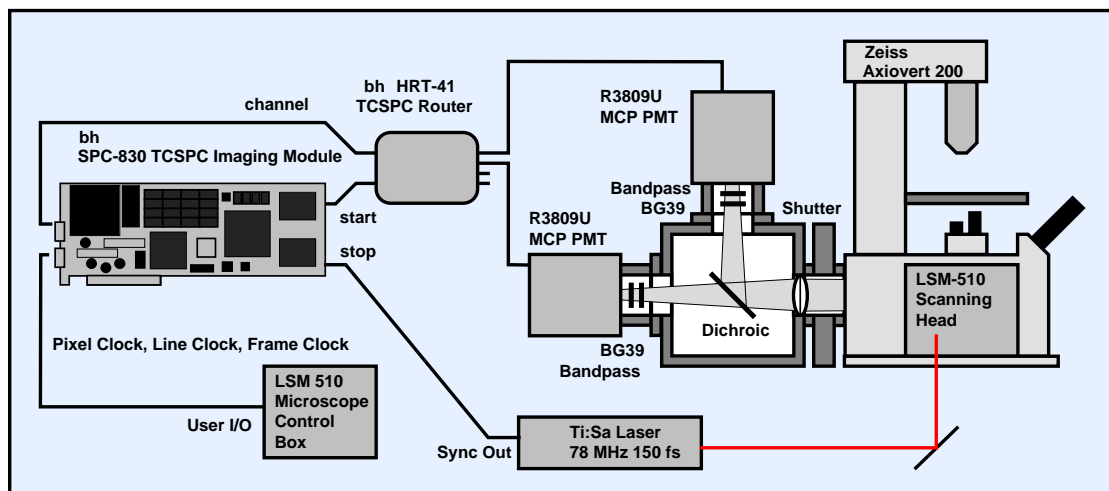


Fig. 4: Setup of the dual-wavelength lifetime microscope (components not to scale)



Fig. 5: Dual R3809U assembly for general application.



Fig. 6: Dual R3809U assembly for Zeiss LSM 510 NDD box

4. RESULTS

The detection system was tested for electronic time resolution and channel separation by sending an attenuated laser beam directly to the detectors. The instrument response function (IRF) at 3kV MCP operating voltage is shown in fig. 7. The IRF width is 28 ps. The electronic channel separation remains better than $1:10^6$ up to a count rate of $1.5 \cdot 10^6 \text{ s}^{-1}$. The optical channel separation of different fluorophores - particularly CFP and YFP - must be expected much lower due to the overlap of the fluorescence spectra.

Fig. 8 shows a cell transfected with CFP only. The cell was excited by two-photon absorption at 860 nm. The two images were obtained in the 480 nm channel and the 535 nm channel, respectively. Due to the long wavelength tail of the CFP fluorescence spectrum [6] a considerable amount of CFP fluorescence is detected in the 535 nm channel. This known

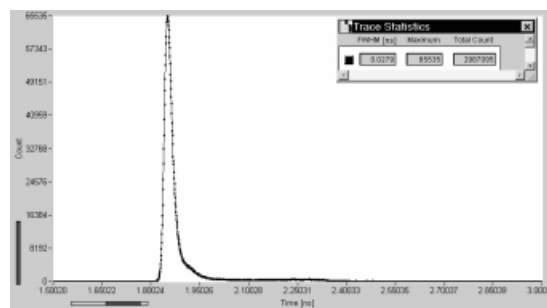


Fig. 7: Instrument response function, 3 kV MCP voltage

problems has significant implications to quantitative FRET measurements that use intensity ratios of the CFP and YFP fluorescence. The single exponential lifetimes averaged over the whole images are 2.28 ns and 2.13 ns, in reasonable agreement with [7]. The decay functions of a 3x3 pixel region around the indicated location are shown right. The decay functions in both wavelength channels are double exponential with two components of 1.2 to 1.3 ns and 2.8 to 2.9 ns. The deviation from a single exponential decay is very small and not discernible in data obtained from single pixels. Although the non-ideal CFP decay does not have severe implications to FRET measurements it should be noted that detailed investigation of the fluorescence decay of the GFP mutants and its dependence on local environment parameters appears indicated.

Fig. 9 shows similar results for a cell transfected with YFP only. Because the YFP is not excited efficiently at 860 nm the brightness scale was stretched by a factor of 22.5 compared to the CFP images. No YFP fluorescence was detected in the 480 nm channel, and the decay curve is single-exponential within the accuracy of the photon statistics.

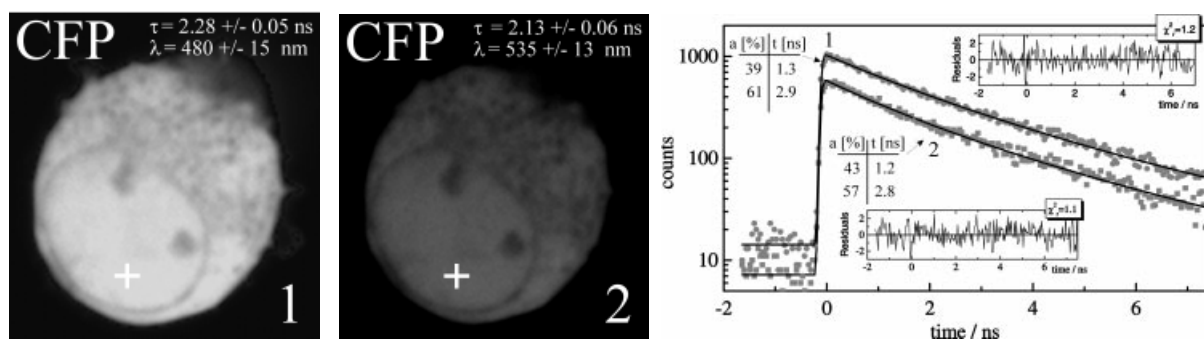


Fig. 8: HEK cell transfected with CFP. Left: 480 nm channel, centre: 535 nm channel. The indicated lifetime is averaged over the whole cell. Right: Decay curves in the selected spot of 3x3 pixels.

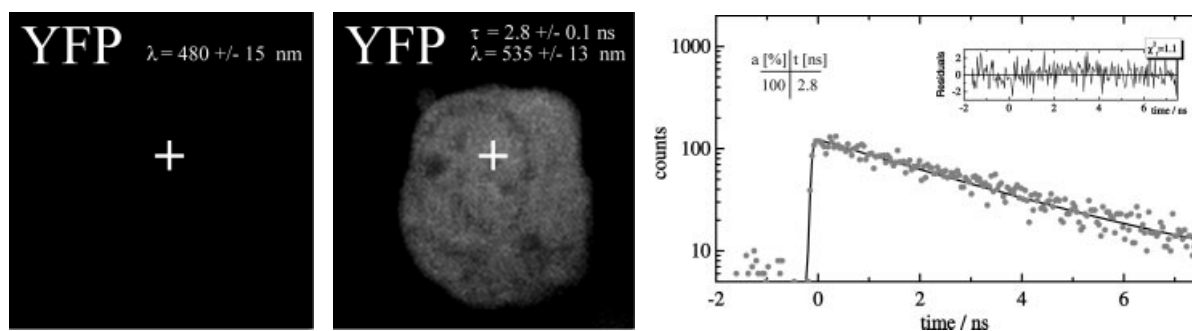


Fig. 9: HEK cell transfected with YFP. Left: 480 nm channel, Centre: 535 nm channel. The indicated lifetime is averaged over the whole cell. Right: Decay curves in the selected spot of 3x3 pixels. Brightness is increased by a factor of 22.5 compared to CFP images

Fig. 10 shows FLIM results for an HEK cell expressing two interacting proteins, which are labeled with CFP and YFP, respectively. FRET is expected in the regions where the proteins are co-localised. The fluorescence was excited by two-photon absorption at 860 nm. The TCSPC images were recorded with 128 x 128 pixels, i.e. with a 4 x 4 binning of the pixels of the regular 512 x 512 LSM 510 scan. The 480 nm (CFP) channel is shown left, the 535 nm (YFP) channel right. Both figures contain a lifetime image with the single-exponential lifetime approximation used as colour, the distribution of the lifetimes in a region of interest, and the fluorescence decay functions in a selected 3x3 pixel area.

The YFP intensity is highest in the regions where the CFP lifetime is shortest. This is a strong indication that FRET occurs between CFP and YFP. A double exponential analysis shows a fast lifetime component of $t_1 = 663$ ps and a

slow one of $t_2 = 2.298$ ns. The intensity coefficients are $a_1 = 0.479$ and $a_2 = 0.521$, respectively. It appears reasonable to relate these components to the quenched and unquenched donor molecules.

Due to the energy transfer from the CFP the YFP fluorescence should actually show an excimer-like decay, i.e. a fast decay component, t_1 , with a lifetime that corresponds to the fast CFP component, and a negative intensity coefficient, a_1 . Although this behaviour can often be observed in cells that have all the CFP and YFP molecules linked directly by a lipid chain [33] no such decay component was found in the cells investigated here. The decay is almost single exponential. The lifetime is 2.7 ns with an 4.5 % contribution of 600 ps. The reason is most likely the overlap of the long wavelength tail of the CFP spectrum into the 535 nm (YFP) channel. Therefore the 535 nm channel contains a considerable fraction of CFP fluorescence, and the positive fast CFP component overcompensates the negative fast YFP component.

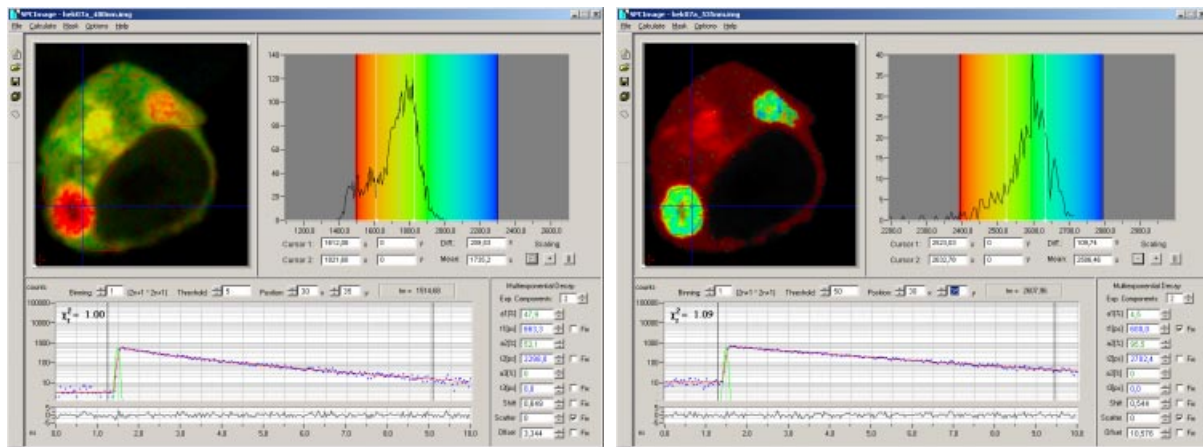


Fig. 10: HEK cell expressing two interacting proteins labeled with CFP and YFP. Left: 480 nm channel. Right: 535 nm channel. Single exponential lifetime images, lifetime distributions in a region of interest, decay functions a in selected pixel, and double exponential fit for selected spot of 3×3 pixels.

Fig 11 shows images which were calculated by fitting a biexponential decay function to the data obtained in the 480 nm (CFP) channel. The images show the lifetime of the fast decay component (left), the lifetime of the slow component (middle), and the ratio of the intensity coefficients a_{fast} / a_{slow} (right) as colour.

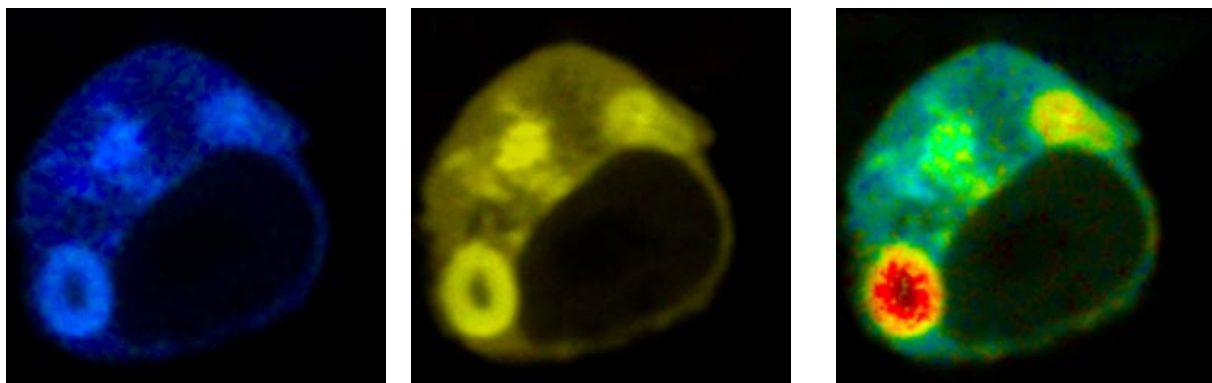


Fig. 11: HEK cell expressing two interacting proteins labeled with CFP and YFP. Left: Lifetime image of the fast decay component, Middle: Lifetime image of the slow decay component, Right: Image of the ratio of coefficients a_{fast} / a_{slow} . The parameters are shown as colour. Colour scale of lifetime is from 500 ps (blue) to 2500 ps (red), colour scale of a_{fast} / a_{slow} is from 0.2 (blue) to 1.0 (red).

The lifetimes of the decay components do not change significantly throughout the image. However, a strong effect is seen in the relative intensity coefficients of the two lifetime components. Although the same general effects are seen in the single exponential lifetimes image of fig. 10 double exponential analysis has the benefit that the relative coefficients represent the relative number of quenched and unquenched molecules, whereas the lifetime of the fast component is related to the average coupling efficiency of the FRET pairs.

For the images shown above 4 x 4 pixels of the regular 512 x 512 pixel scan of the LSM 510 were binned to get enough time bins and enough photons per pixel to run a double-exponential decay analysis. However, the SPC-830 module is able to record single wavelength lifetime images with 1024 x 1024 pixels and dual, triple or quadruple wavelength lifetime images with 512 x 512 pixels. An example is shown in fig. 12. It shows a 16 μm cryostat section of a mouse kidney (Molecular Probes, F-24630) stained with Alexa Fluor 488 WGA, Alexa Fluor 568 phalloidin, and DAPI. The sample was excited by two-photon excitation at 860 nm. Fig. 12 (left) shows a 1024 x 1024 pixel image containing the photons of both wavelength channels. Although the fluorophores are not excited efficiently at 860 nm the image clearly shows different lifetimes.

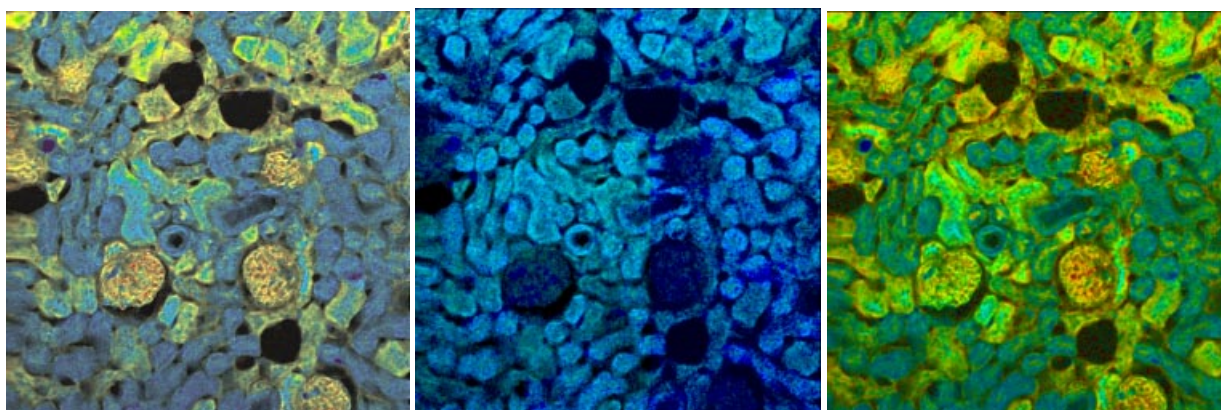


Fig. 12: Mouse kidney sample stained with Alexa Fluor 488 WGA, Alexa Fluor 568 phalloidin, and DAPI. Colour represents lifetime, blue to red = 750 to 2250 ps. Left: 1024 x 1024 pixel image containing the photons of both wavelength channels, Middle: 512 x 512 image of 488 nm channel, Right: 512 x 512 image of 535 nm channel

Fig. 12, middle and right, show two 512 x 512 pixel images obtained in the 488 nm and in the 535 nm channel. The 488 nm image shows mainly the Alexa Fluor 488 fluorescence originating from labeled elements of the glomeruli and convoluted tubes. Therefore the lifetime is almost constant. In the 535 nm channel all three fluorophores are detected. Alexa Fluor phalloidin stained the filamentous actin prevalent in the glomeruli and the brush border. The signals overlap in this channel but can be separated by their lifetime.

5. CONCLUSIONS

TCSPC imaging delivers high resolution lifetime images simultaneously in several wavelength intervals. Compared to consecutive single wavelength imaging the counting efficiency is multiplied by the number of detection channels. The technique can be used to image the donor and the acceptor fluorescence in FRET systems simultaneously and to resolve the multi-exponential decay of the donor fluorescence. Other possible applications are autofluorescence lifetime imaging of tissue and lifetime imaging of cells or tissue containing several fluorophores with environment-dependent lifetimes.

6. REFERENCES

1. Van Zandvoort, M.A.M.J., de Grauw, C.J., Gerritsen, H.C., Broers, J.L.V., Egbrink, M.G.A. Ramaekers, F.C.S., Slaaf, D.W. Discrimination of DNA and RNA in cells by a vital fluorescent probe: Lifetime imaging of SYTO13 in healthy and apoptotic cells. *Cytometry* 47, 226-223 (2002)

2. J-P. Knemeyer, N. Marmé, M. Sauer, Probes for detection of specific DNA sequences at the single molecule level. *Anal. Chem.* 72 (2000) 3717-3724
3. J.R. Lakowicz, H. Szmajcinski, Fluorescence-lifetime based sensing of pH, Ca²⁺, and glucose. *Sens. Actuator-Chem.* 11, 133-134 (1993)
4. H.C. Gerritsen, R. Sanders, A. Draaijer, Y.K. Levine, Fluorescence lifetime imaging of oxygen in living cells. *J. Fluoresc.* 7, 11-16
5. W. Becker, K. Benndorf, A. Bergmann, C. Biskup, K. König, U. Tirplapur, Th. Zimmer, FRET Measurements by TCSPC laser scanning microscopy. *Proc. SPIE*, 4431, 94-98, (2001)
6. M. Elangovan, R.N. Day, A. Periasami, Nanosecond fluorescence resonance energy transfer-fluorescence lifetime imaging microscopy to localize the protein interactions in a single cell. *J. Microsc.* 205 (2002) 3-14
7. R. Pepperkok, A. Squire, S. Geley, P.I.H. Bastiaens, Simultaneous detection of multiple green fluorescent proteins in live cells by fluorescence lifetime imaging microscopy. *Curr. Biol.* 9, 269-272 (1999)
8. K. König, C. Peuckert, I. Riemann, U. Wollina, (2002) Optical tomography of human skin with subcellular resolution and picosecond time resolution using intense near infrared femtosecond laser pulses. *Proc. SPIE* 4620, 191-201 (2002)
9. D. Schweitzer, A. Kolb, M. Hammer, E. Thamm, Basic investigations for 2-dimensional time-resolved fluorescence measurements at the fundus. *Int. Ophthalmol.* 23, 399-404 (2001)
10. J.G. White, W.B. Amos, M. Fordham, An evaluation of confocal versus conventional imaging of biological structures by fluorescence light microscopy. *J Cell Biol* 105, 41-48 (1987).
11. W. Denk, J.H. Strickler, W.W. Webb, Two-photon laser scanning fluorescence microscopy. *Science* 24 (1990) 73-76
12. J. Pawley (Editor), *Handbook of biological confocal microscopy*. Plenum, New York (1995)
13. A. Periasami, M. Elangovan, H. Wallrabe, J.N. Demas, M. Barroso, D.L. Brautigan, R.N. Day, *Methods in cellular imaging* (ed. by A. Periasami), Oxford University Press, New York
14. B. Herman, *Fluorescence Microscopy*, 2nd. edn. Springer-Verlag, New York 1998
15. K. König, Multiphoton microscopy in life sciences. *J. Microsc.* 200, 83-104 (2000)
16. P.T.C. So, T. French, W.M. Yu, K.M. Berland, C.Y. Dong, E. Gratton, Time-resolved fluorescence microscopy using two-photon excitation. *Bioimaging* 3 (1995) 49-63
17. K. Carlsson, A. Liljeborg, Confocal fluorescence microscopy using spectral and lifetime information to simultaneously record four fluorophores with high channel separation. *J. Microsc.* 185 (1997) 37-46
18. K. Carlsson, A. Liljeborg, Simultaneous confocal lifetime imaging of multiple fluorophores using the intensity-modulated multiple-wavelength scanning (IMS) technique. *J. Microsc.* 191 (1998) 119-127
19. J.R. Lakowicz, K. Berndt, Lifetime-selective fluorescence lifetime imaging using an rf phase-sensitive camera. *Rev. Sci. Instrum.* 62, 1727-1734 (1991)
20. P.T.C. So, T. French, E. Gratton, A frequency domain microscope using a fast-scan CCD camera. *Proc. SPIE* Vol. 2137/83
21. A. Squire, P.J. Verveer, P.I.H. Bastiaens: Multiple frequency fluorescence lifetime imaging microscopy. *J. Microsc.* 197, 136-149 (2000).
22. M. Straub, S. W. Hell, Fluorescence lifetime three-dimensional microscopy with picosecond precision using a multifocal multiphoton microscope. *Appl. Phys. Lett.* 73 (1998) 1769-1771
23. M.J. Cole, J. Siegel, R. Dowling, M.J. Dayel, D. Parsons-Karavassilis, P.M. French, M.J. Lever, L.O. Sucharov, M.A. Neil, R. Juskaitas, T. Wilson, Time-domain whole-field lifetime imaging with optical sectioning. *J. Microsc.* 203 (2001) 246-257
24. E.P. Buurman, R. Sanders, A. Draaijer, H.C. Gerritsen, J.J.F. van Veen, P.M. Houpt, Y.K. Levine, Fluorescence lifetime imaging using a confocal laser scanning microscope. *Scanning* 14, 155-159 (1992).
25. J. Syrtsma, J.M. Vroom, C.J. de Grauw, H.C. Gerritsen, Time-gated fluorescence lifetime imaging and microvolume spectroscopy using two-photon excitation. *J. Microsc.* 191, 39-51 (1998)
26. I. Bugiel, K. König, H. Wabnitz, Investigations of cells by fluorescence laser scanning microscopy with subnanosecond resolution. *Lasers in the Life Sciences* 3, 47-53 (1989)
27. H. Brismar, B. Ulfhake, Fluorescence lifetime measurements in confocal microscopy of neurons labeled with multiple fluorophores. *Nat. Biotech.* 15, 373-377 (1997)

28. W. Becker, A. Bergmann, K. Koenig, U. Tirlapur, Picosecond fluorescence lifetime microscopy by TCSPC imaging. Proc. SPIE 4262, 414-419 (2001)
29. M. Köllner, J. Wolfrum, How many photons are necessary for fluorescence-lifetime measurements? Phys. Chem. Lett. 199-204 (1992)
30. G.H. Patterson, D.W. Piston, Photobleaching in two-photon excitation microscopy. Biophys. J. 78, 2159-2162 (2000)
31. D.V. O'Connor, D. Phillips, Time Correlated Single Photon Counting, Academic Press, London (1984)
32. W. Becker, A. Bergmann, H. Wabnitz, D. Grosenick, A. Liebert, High count rate multichannel TCSPC for optical tomography. Proc. SPIE 4431, 249-254 (2001)
33. Wolfgang Becker, Axel Bergmann, Christoph Biskup, Thomas Zimmer, Nikolaj Klöcker, Klaus Benndorf, Multi-wavelength TCSPC lifetime imaging. Proc. SPIE 4620, 79-84, (2002)
34. Ballew, R.M., Demas, J.N., An error analysis of the rapid lifetime determination method for the evaluation of single exponential decays. Anal. Chem. 61 (1989) 30-33
35. K. Carlsson, J.P. Philip, Theoretical investigation of the signal-to-noise ratio for different fluorescence lifetime imaging techniques. Proc. SPIE 4622, 70-78 (2002)
36. H.C. Gerritsen, M.A.H. Asselbergs, A.V. Agronskaia, W.G.J.H.M van Sark. Fluorescence lifetime imaging in scanning microscopes: acquisition speed, photon economy and lifetime resolution. J. Microsc. 206, 218-224 (2002)
37. Hidehiro Kume (Chief Editor), Photomultiplier Tube, Hamamatsu Photonics K.K., 1994
38. HRT-41, HRT-81, HRT-82 Routing Devices, Operating Manual. Becker & Hickl GmbH, www.becker-hickl.com
39. SPC-134 through SPC-730 TCSPC Modules, Operating Manual and TCSPC Compendium. Becker & Hickl GmbH, www.becker-hickl.com

Correspondence:
Wolfgang Becker
becker@becker-hickl.com